Electronic Supplementary Information

Waxy Rice Amylopectin towards Stretchable Elastic Conductive Hydrogel for Human Motions Detection

Xiaodong Song, Xiaxin Qiu, Xiaowen Huang, Yaqing Tu, Qiuhua Zhao* Ruyi Sun* and Lidong Zhang*

School of Chemistry and Molecular Engineering, East China Normal University, Shanghai, 200241, People's Republic of China.

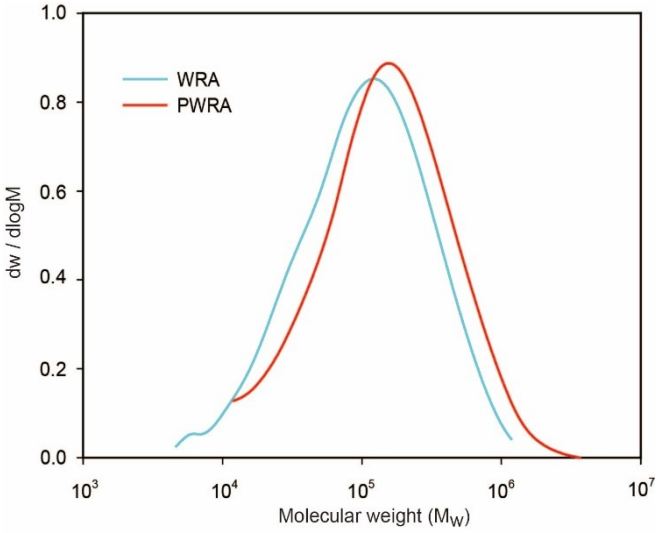

Fig. S1. GPC analysis. Molecular weight distribution curves of WRA and PWRA.

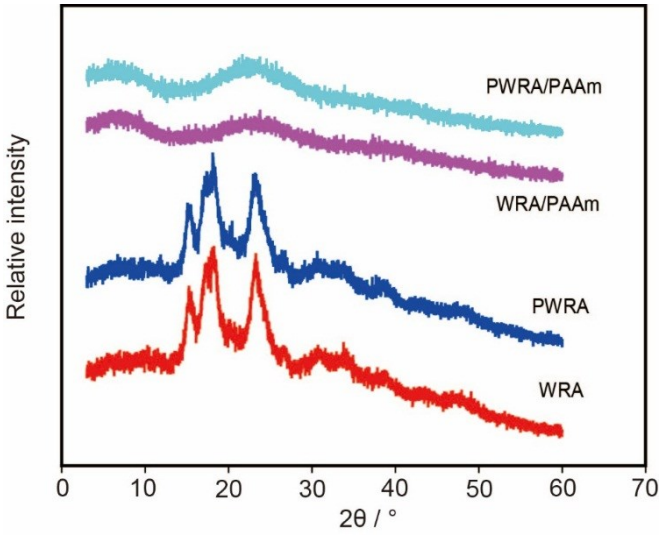

Fig. S2. Physical structure analysis. XRD profiles of WRA, PWRA, WRA/PAAm and PWRA/PAAm.

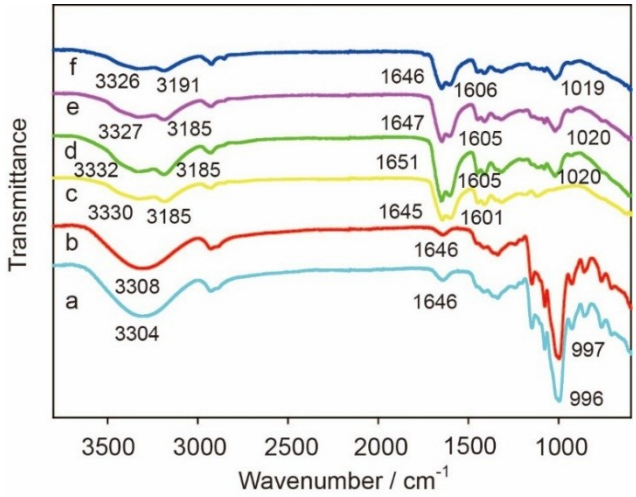

Fig. S3. Chemical structure analysis. FT-IR spectra of (a) WRA, (b) PWRA, (c) PAAm, (d,e,f) PWRA/PAAm hydrogels. (d) PWRA: AAm = 0.25; (e) PWRA: AAm = 0.5; (f) PWRA: AAm = 1.

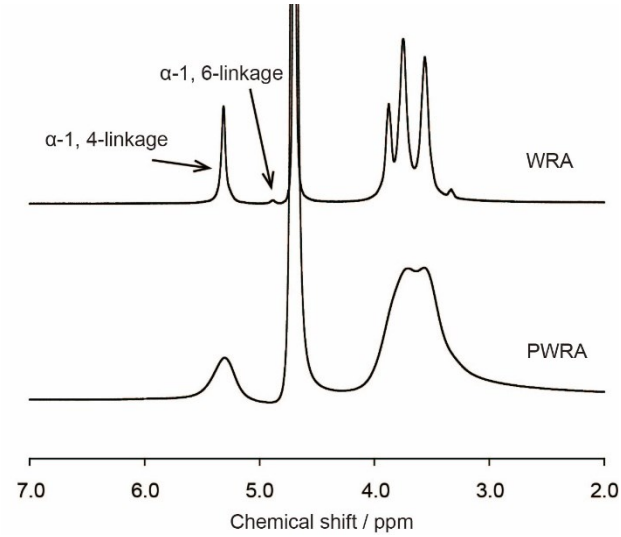

Fig. S4. ^{1}H NMR spectra of WRA and PWRA. Peaks at 5.31 ppm and 4.88 ppm corresponded to anomeric protons of α-1,4 and α-1,6 glycosidic bonds (Food Chemistry, 2019, 294, 440-447).

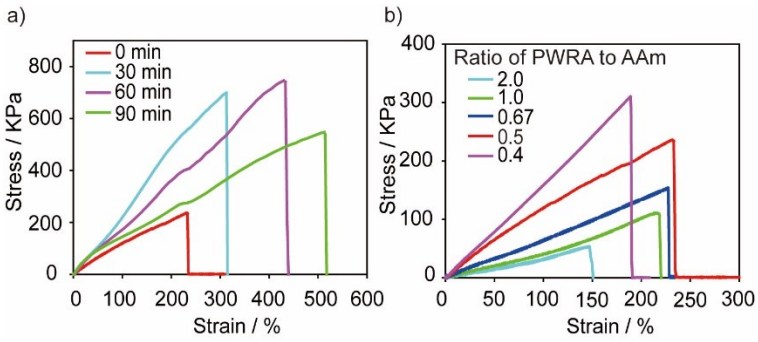

Fig. S5. Influencing factors on the mechanical properties of the hydrogels. (a) Dehydration time effects. (b) PWRA to AAm weight ratio effects.

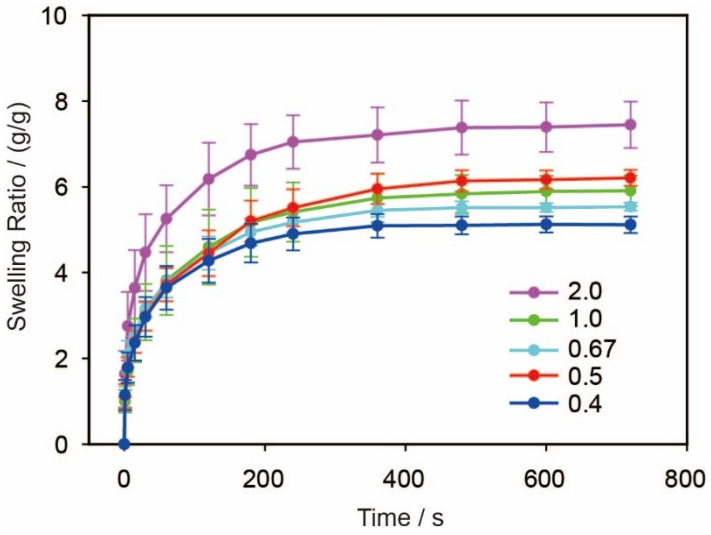

Fig. S6. Swelling ratio of PWRA/PAAm hydrogel. All hydrogel samples were dried completely in an oven at 40 °C before testing. The swelling ratio (SR) of the hydrogels at room temperature

were tested. The SR is defined by the following equation: SR = $(W_s - W_d)/W_d$, where W_s is the weight of wet hydrogel, and W_d is the dry weight of hydrogel.

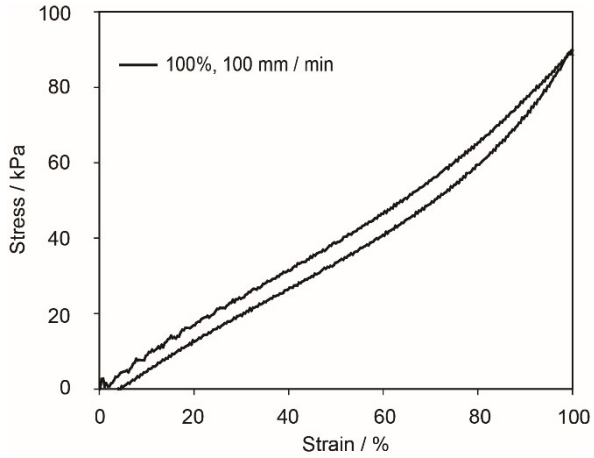

Fig. S7. The hysteresis curve of PWRA/PAAm hydrogel. The hydrogel was stretched to 100% strain, and unloaded to allow the hydrogel to recover its original length. The result indicated that the hydrogel was highly elastic.

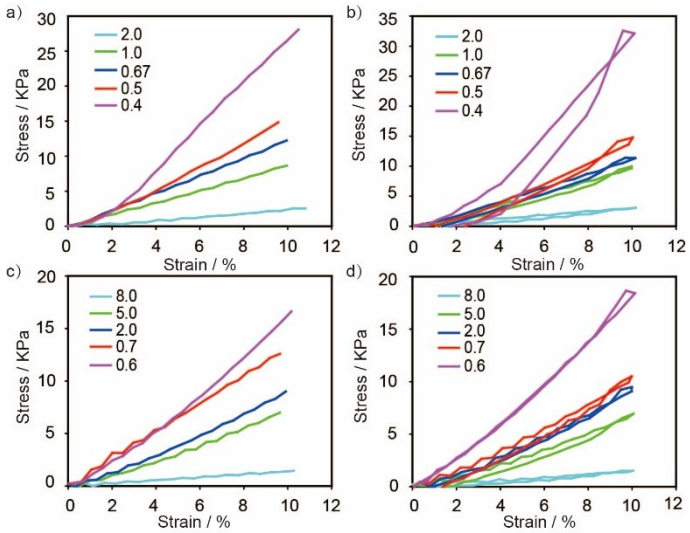

Fig. S8. Compression test of hydrogels at different weight ratios of PWRA to PAAm. (a) Stress-strain profiles of hydrogel before dialysis at 10% strain, and (b) its loading/unloading cycle profiles. (c) Stress-strain profiles of hydrogel after dialysis, and (d) its loading/unloading cycle profiles. The loading/unloading speed was constant at 10 mm/min. The modulus was calculated according to the profiles in Fig S7a, which indicated that with the weight ratio of PWRA to PAM being decreased from 2.0 to 0.4, the modulus increased from 24.6 KPa, 83.4 KPa, 169.2 KPa, 212.9 KPa to 275.5 KPa, respectively.

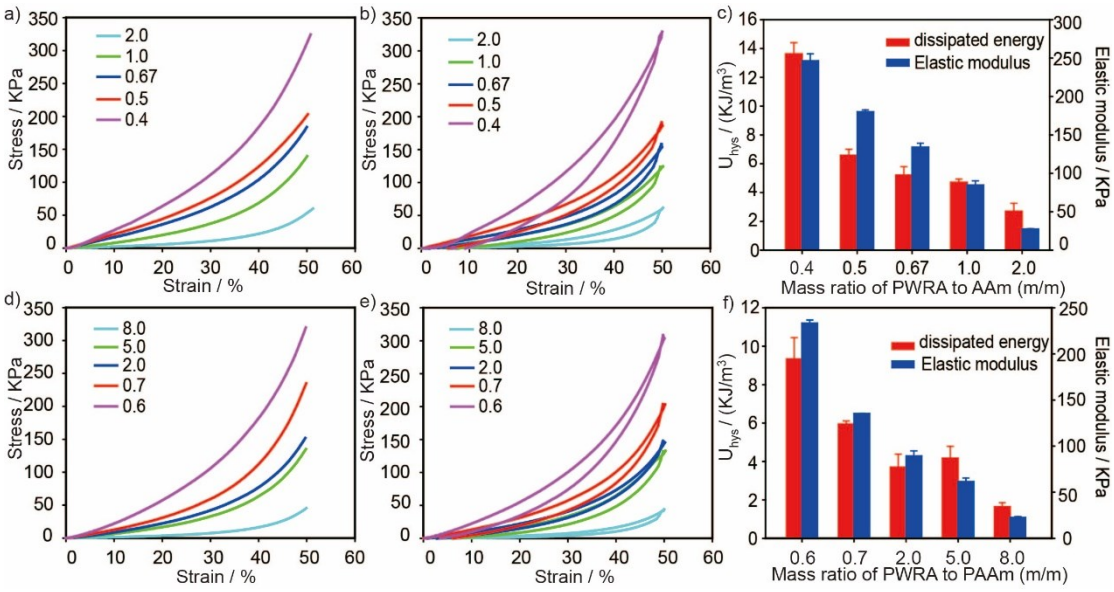

Fig. S9. Compression test of hydrogels at different weight ratios of PWRA to PAAm under 50% strain. (a) Stress-strain profiles of the hydrogel before dialysis at 50% strain, and (b) its loading/unloading cycle profiles, and (c) the dissipated energies and elastic modulus. (d) Stress-strain profiles of hydrogel after dialysis at 50% strain, and (e) its loading/unloading cycle profiles, and (f) the dissipated energies and elastic modulus. The loading/unloading speed was constant at 10 mm/min.

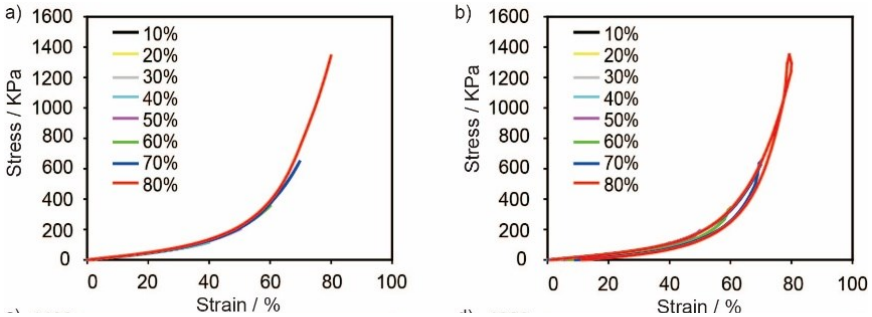

Fig. S10. Compression test of PWRA/PAAm at 80% strain**.** (a) Stress-strain profiles of the hydrogel before dialysis at 80% strain, and (b) its loading/unloading cycle profiles. The compressive speed was constant at 10 mm/min.

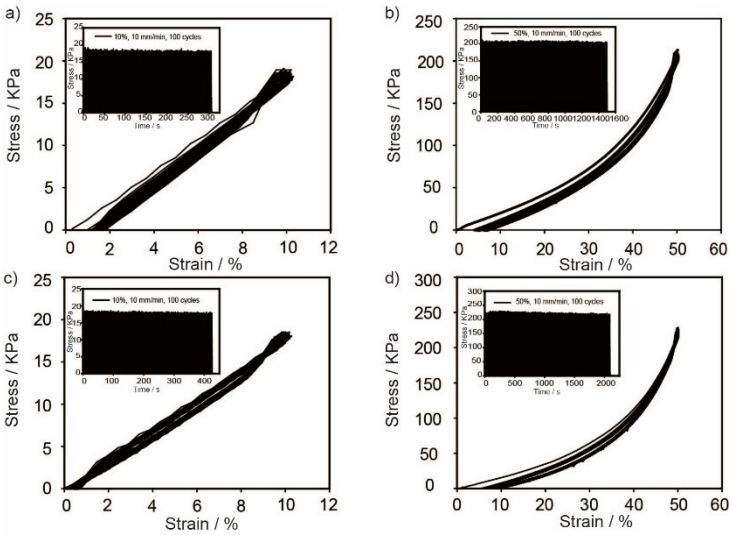

Fig. S11. Loading-unloading curves of PWRA/PAAm hydrogel. (a) Loading/unloading cycles of the hydrogel **before** dialysis at 10% strain, and (b) at 50% strain. (c) Loading/unloading cycles of the hydrogel **after** dialysis at 10% strain, and (d) at 50% strain. Inset shows stress-time profiles indicating the stress variation during the compressive cycling testing. The loading/unloading speed was ± 10 mm/min and 100 cycles were proceeded for one sample.

Operation: PWRA/PAAm hydrogel was cut to a rectangle strip (5 mm x 5 mm x 3 mm), and mounted on a mechanical tensile tester for reversible stretching. In each cycle, the strip was compressed to 10% or 50% strain at a rate of 10 mm/min; then the unloading process started at the same rate until recovering to the original gauge length (3 mm).

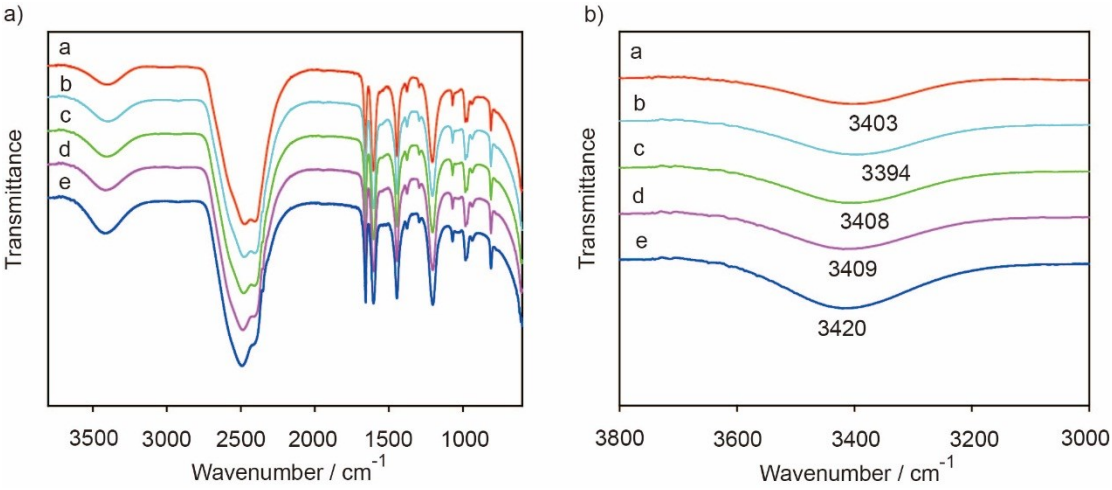

Fig. S12. FTIR spectra of PWRA and AAm mixtures in 0.1 mL D_2O. The mixture was added LiBr to remove hydrogen bonding interactions. The weight ratio of PWRA to AAm was 0.5. LiBr content was increased from 0, 40, 100, 200, to 400 mg / mL, respectively from a to e profiles. (a) full spectrum of each sample, and (b) zoom-in spectrum of each sample.

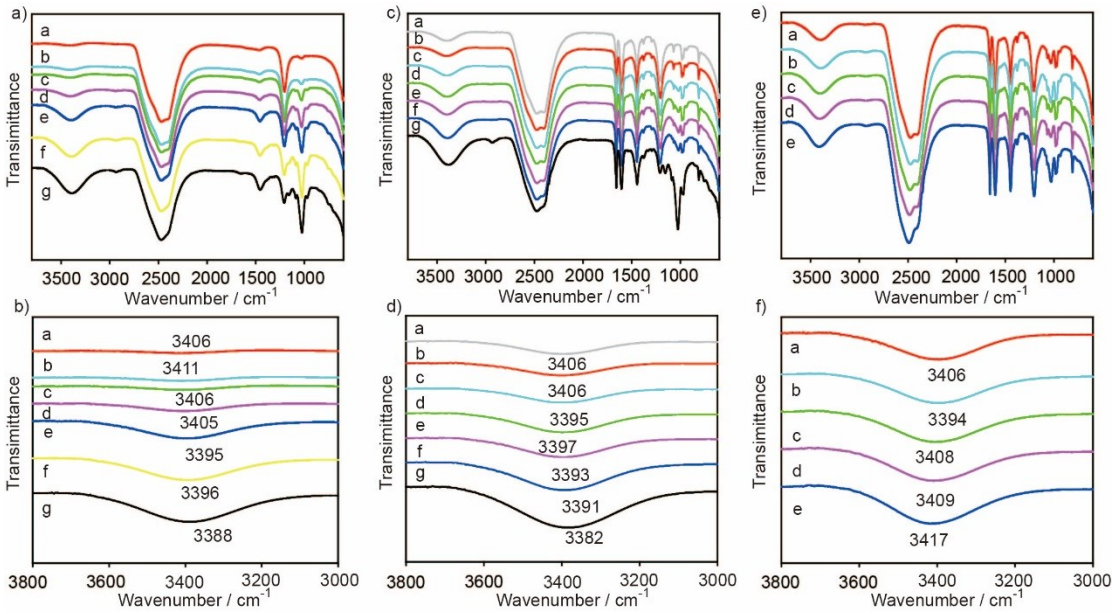

Fig. S13. FT-IR spectroscopy. (a,b) WRA in 0.1 mL D_2O. WRA content was 25, 50, 100, 200, 400, 600, and 800 mg / mL from a to g. (a)full spectrum, (b) Zoom-in spectrum. (c,d) WRA and AAm mixture in 0.1 g D_2O. Keeping AAm content constant at 200 mg / mL, and WRA content was increased from 0, 25, 50, 100, 200, 400 and 800 mg / mL, respectively from a to g. (e, f) WRA and AAm mixture in 0.1 mL D_2O with different proportions of LiBr. AAm content was constant at 200 mg / mL, and WRA content was constant at 100 mg / mL. LiBr was increased from 0, 40, 100, 200, to 400 mg / mL, respectively. (b), (d) and (f) demonstrating the focused observation of (a), (c) and (e) spectra.

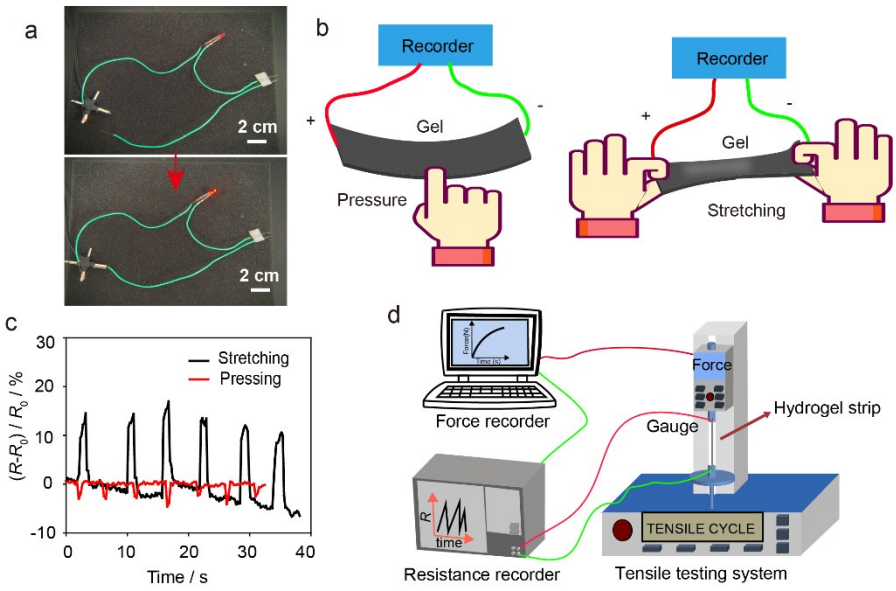

Fig. S14. Conductivity and pressure sensing. (a) A small piece of PWRA/PAAm hydrogel was used as a conductive wire to turn light on. (b) Schematics of the resistance change of hydrogels under external forces. (c) Curves of resistance variation of the hydrogel by external force. (d) Experimental setup to quantitatively measure the relationship between external forces and electric resistances.

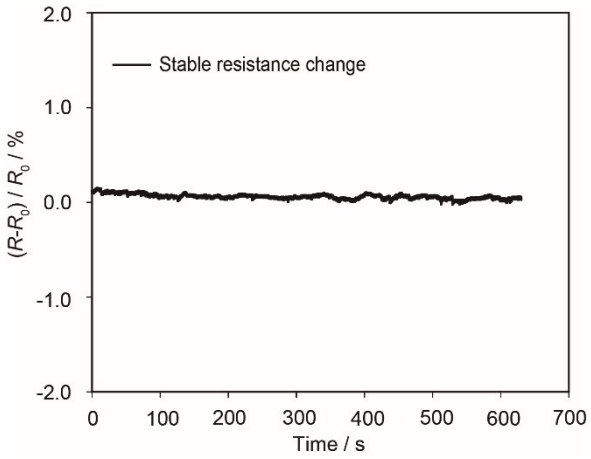

Fig. S15. Resistance variation-time curve of PWRA/PAAm hydrogel. The hydrogel was tested without external force was loaded. The result was used as a background reference for the analysis of external force effects on the resistance variation (ΔR).

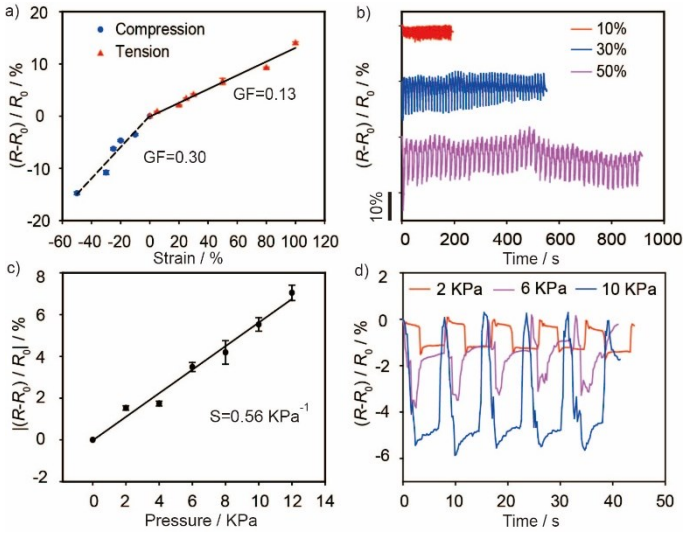

Fig. S16. Pressure sensitivity. (a) Relative resistance variation of PWRA/PAAm hydrogel as a function of tension strain (red triangles) and compression strain (blue circles). (b) Relative resistance variation during the loading/unloading at different compression strains. The compressive speed was constant at ±30 mm/min. (c) Relative resistance variation versus pressure for the hydrogel sensor. (d) Relative resistance variation as function of time under different pressures. The compressive speed was constant at ±10 mm/min.

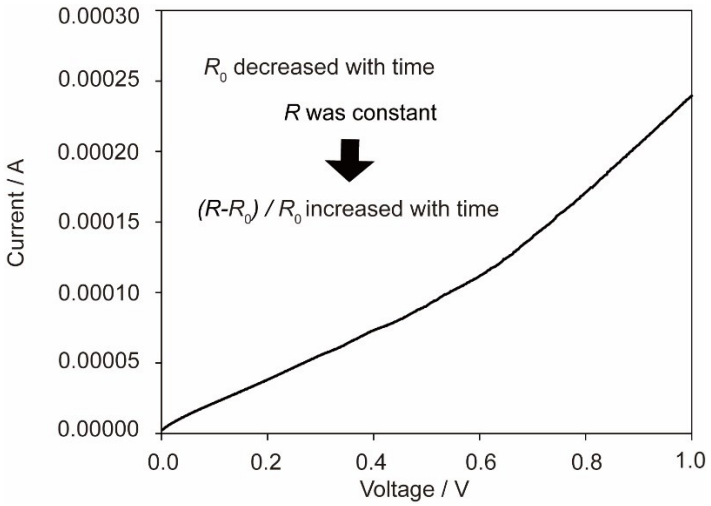

Fig. S17. Current-voltage curves. Increasing the voltage resulted in the increase of the current; however, the current increased not linearly, but more rapidly as the voltage was more than 0.6 V. This result indicated that the resistance (R_0) of the hydrogel decreased with time. When R was constant, $\Delta R = (R - R_0) / R_0$ would increase with time.

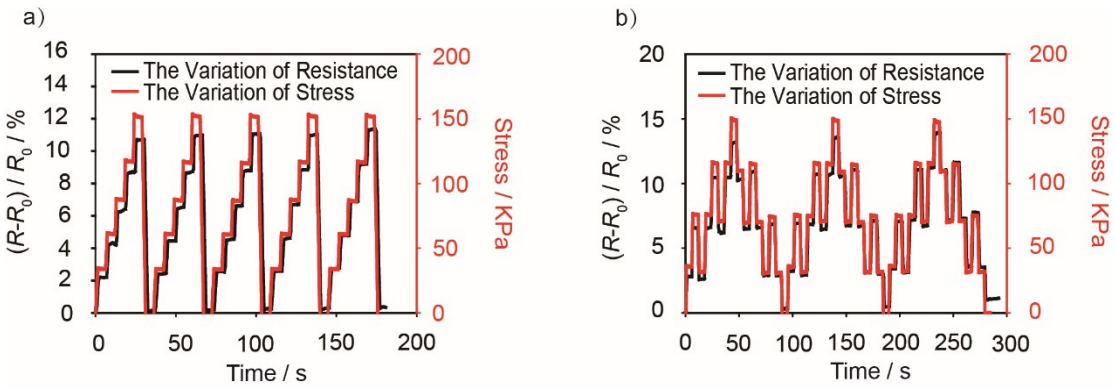

Fig. S18. Relative resistance and stress variation with time during tensile testing. (a) Elongation: 20%, 40%, 60%, 80%, and 100%; stretching speed: +100, +150, +200, +250, +300, and then -300 mm / min, respectively; residence time: 5s. (b) Elongation: 20%, 50%, 80%, and 100%; stretching speed: ±200 mm/min; residence time: 5s.

Legends for Supplementary Movies

Movie S1. Tensile test of stretchable and elastic PWRA/PAAm hydrogel. The video is at four times the real speed.

Movie S2. Weight-lifting test showing the robust and elastic capability of PWRA/PAAm hydrogel. The video is at four times the real speed.

Movie S3. Making a sheet of PWRA/PAAm hydrogel into a helical shape or a knot. The video is at

two times the real speed.

Movie S4. Demonstration on the pressure-sensitive PWRA/PAAm hydrogel. The electric signals generated with an apparent regularity depending on the external force. The video is at five times the real speed.